Article:
Zhao, Y, Qian, K, Sheng, B et al. (5 more authors) (2022) Adaptive Cooperative Control Strategy for a Wrist Exoskeleton using Model-based Joint Impedance Estimation. IEEE/ASME Transactions on Mechatronics. ISSN 1083-4435

https://doi.org/10.1109/TMECH.2022.3211671

Adaptive Cooperative Control Strategy for a Wrist Exoskeleton using Model-based Joint Impedance Estimation

Yihui Zhao, Kun Qian, Sheng Bo, Zhiqiang Zhang, *Member, IEEE,* Zhenhong Li, *Member, IEEE,* Gu-Qiang Li, Abbas A. Dehghani-Sanij, *Member, IEEE,* and Shengquan Xie, *Senior Member, IEEE*

***Abstract*—Wrist rehabilitation exoskeletons have gained much attention over the last decades, striving to restore motor functions for patients with neuromuscular disorders. Electromyography (EMG) signal has been employed to estimate the motion intention to achieve interactive training schemes. However, it is a challenging task to estimate the joint impedance in real-time, as it is a crucial parameter for control of exoskeletons. This paper proposes an adaptive cooperative control strategy for a wrist exoskeleton based on a real-time joint impedance estimation approach. By explicitly interpreting the underlying transformation in the muscular and skeletal systems, the proposed approach estimates the motion intention and the joint impedance of a human subject simultaneously without additional calibration procedures and regulates the training trajectories and assistance accordingly. Results indicate the proposed method outperforms other training protocols, including the trajectory tracking control and the fixed cooperative control. The proposed control strategy provides an additional 66.25% motion deviation when estimated joint torque increases 12.36%, which enhances the training effectiveness and the interaction safety and promotes subjects' active engagement.**

***Index Terms*—Wrist rehabilitation robot, electromyography, musculoskeletal model, joint impedance, adaptive cooperative control strategy.**

I. Introduction

WRIST rehabilitation exoskeletons have been studied in the last decades, striving to restore the motor function for patients with neuromuscular disorders [1]. The interactive training schemes have gained much attention as they encourage the patients' participation and promote motor recovery [2]–[4]. For the interactive training schemes, the accuracy and reliability of motion intention estimation are paramount for such control strategies.

Electromyography (EMG) signal offers a promising solution given its ability to decode motion intention at the spinal cord level and can be detected prior to the initiation of movement [5], [6]. State-of-the-art EMG-based approaches mainly employ regression algorithms that map EMG signals to the motion intention through numerical functions [7]. For example, Sierotowicz *et al.* presented a soft glove with a control scheme to estimate motion intention based on the ridge regression algorithm [8]. Wu *et al.* used a Gaussian radial basis function network to estimate the motion intention for an adaptive controller in the upper limb rehabilitation robot [9]. However, the regression algorithms require abundant training data and are sensitive to movement artefacts. Additionally, they fail to decouple the joint impedance property when trained by the EMG signal and kinetic/kinematic data. In fact, the joint impedance can vary substantially while kinetic/kinematic outputs stay same. The exoskeleton should adapt to the joint impedance to ensure the comfortable coordinated motion in the interactive training scheme [10], [11].

To evaluate joint impedance, experimental measurements are commonly conducted using the perturbation techniques [12]–[15]. However, it becomes a challenging task to estimate the joint impedance with the wearable exoskeleton in real-time, as the joint impedance is influenced by muscle activation patterns significantly. Efforts are made into integrating the joint impedance with control strategies via EMG signals [16], [17]. For instance, Antuvan *et al.* modulated the stiffness parameter of the controller using the index of muscle co-contraction around the joint [18]. Wu *et al.* utilised a piecewise function to relate the stiffness of the robotic manipulator to EMG signals in the demonstration learning task [19]. Zeng *et al.* also utilised the EMG signal to map the joint impedance profile into robot impedance controller [20]. These methods require rich and diverse experimental data for calibration, which increases experimental and computational costs.

To address these issues, a musculoskeleltal model has been proposed to estimate the motion intention and joint impedance simultaneously. The model-based approach explicitly reveals the underlying non-linear transformation among the muscular and skeletal systems. Pfeifer *et al.* employed an EMG-driven model-based approach to estimate the knee stiffness which coincides well with the conventional perturbation method [21].

This work was supported in part by U.K. EPSRC under Grant EP/S019219/1 and Grant EP/V057782/1. (Corresponding authors:Sheng Quan Xie.)

Yihui Zhao, Kun Qian, Zhiqiang Zhang, and Zhenhong Li are with the School of Electronic and Electrical Engineering, University of Leeds, Leeds LS2 9JT, U.K (E-mails: el14yz@leeds.ac.uk; el14kq@leeds.ac.uk; Z.Zhang3@leeds.ac.uk; z.h.li@leeds.ac.uk).

Sheng Bo is with the School of Mechatronic Engineering and Automation, Shanghai University, 99 Shangda Road, Baoshan District, 200444, Shanghai, China, Email: shengbo@shu.edu.cn.

Gu Qiang Li is with the School of Rehabilitation Medicine, Binzhou Medical University, Yantai 264100, China (e-mail: 951656857@qq.com, email: lgq100@bzmc.edu.cn).

Abbas Dehghai-Sanij is with the School fo Mechanical Engineering, University of Leeds, Leeds LS2 9JT, UK (email: A.A.Dehghani-Sanij@leeds.ac.uk).

Sheng Quan Xie is with the School of Electronic and Electrical Engineering, University of Leeds, Leeds LS2 9JT, UK., also collaboration with the Institute of Rehabilitation Engineering, Binzhou Medical University, Yantai 264033, China (email: s.q.xie@leeds.ac.uk).

Zonnino *et al.* utilised a model-based approach to simulate the wrist joint impedance profiles in active and passive conditions [22]. However, it is unclear if the model-based approach can be generalised to estimate the joint impedance in real time when it is implemented for robot-aided wrist rehabilitation.

In this paper, we proposed an adaptive cooperative control strategy for a wrist exoskeleton using the model joint impedance estimation method. A wrist EMG-driven musculoskeletal model is first developed with the consideration of wrist primary muscles. The wrist exoskeleton is adaptively regulated in response to the instantaneous muscular efforts and joint impedance profiles. The contributions of this paper include: 1) by explicitly imitating the underlying transformation in the muscular and skeletal systems, the model-based approach estimates the joint torque and joint impedance simultaneously without additional calibration procedures. 2) A new adaptive admittance controller is proposed based on the proposed joint impedance estimation approach to regulate the training trajectory and robot's assistance, and 3) the integration and performance evaluation of the EMG-driven model-based approach and the interactive control strategy for robot-aided wrist rehabilitation. The experiments are conducted on 12 healthy subjects. Results indicate the proposed method outperforms other training schemes, including trajectory tracking control and fixed cooperative control. The proposed control strategy provides an additional 66.25% deviation when estimated joint torque increases 12.36%.

The remaining sections of this paper are organised as follows. Section II details the methodologies for real-time estimation of joint impedance. The implementation of model-based control strategy and experimental protocols are also presented. Section III presents the results of the experimental work. The validation of the model-based joint stiffness estimation and the performance of the adaptive cooperative control strategy are discussed in section IV. The final section draws the conclusion.

II. Methods

A. Wrist exoskeleton

The wrist exoskeleton is developed by the intelligent Rehabilitation Robotics Center at Leeds [23]. Fig. 1 illustrates the wrist exoskeleton which consists of a customised frame, two Festo Fluidic muscles and the sensory system. The pneumatic muscles are used as actuators to drive the exoskeleton in the flexion/extension movement. Each muscle has the effective length of $9\,\mathrm{cm}$ and the maximum contraction length of $1.8\,\mathrm{cm}$, which results in the maximum range of motion (RoM) of $\pm$ 30 degree. The compliance of pneumatic muscle could improve the system's flexibility, safety, and comfort of the human-machine system. Moreover, the muscle has advantages such as the simple structure, light weight, and high power-weight ratio, compared with conventional electric motors [24], [25]. The sensory system includes two load cells connected in line with the pneumatic muscles respectively. A potentiometer aligned with rotation centre is utilised as an angle sensor. Two proportional pressure regulators are used for pressure control of two muscles respectively. All sensors are communicated with the NI-myRIO controller. A custom LabVIEW program is designed to process the sensing information and the proposed model-based control strategy.

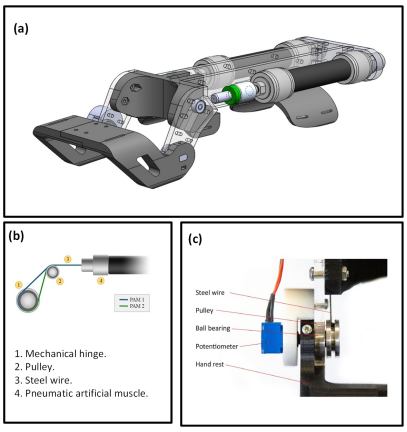

Fig. 1. Mechanical configuration of the wrist exoskeleton. PAM is the abbreviation of pneumatic artificial muscle. (a) The CAD of the wrist exoskeleton. (b) The configuration of steel wires enables flexion/extension movement. (c) Sensory system.

B. Estimation of wrist joint impedance

To estimate the joint impedance, we first develop the EMG-driven musculoskeletal model for the wrist joint. This is because the musculoskeletal model should be optimised in order to obtain the subject-specific physiological parameters. The estimated joint torque is also utilised for the adaptive cooperative control strategy.

The envelop of the sEMG signals (i = 1... 5) are first obtained by filtering the raw signal using a 4^{th} order Butterworth band-pass filter (pass band at $20\,\mathrm{Hz}$ and $450\,\mathrm{Hz}$). The filtered signals are fully rectified and low-pass filtered by a 4^{th} order Butterworth low-pass filter at a corner frequency of 4 Hz. The low-pass filtered signal is then normalised by the maximum voluntary contraction (MVC), results in the enveloped signal $u_i(t)$ (ranged between 0 and 1). Then a non-linear equation is used to obtain the muscle activation $a_i(t)$ from the enveloped signal, which can be written as [26]:

$$a_i(t) = \frac{e^{Au_i(t)} - 1}{e^A - 1} \tag{1}$$

where A is the non-linear shape factor that has the range between 0.001 and -3.

The muscle-tendon model is modelled as an elastic tendon connected in series with a muscle fibre, of which the relationship between muscle fibre and tendon is written as:

$$l_i^m = (k_i l_i^{mt} - l_i^t)\cos^{-1}\phi_i \tag{2}$$

where l_i^m, l_i^{mt} and l_i^t represent the muscle fibre length, muscle-tendon length and tendon length. The muscle-tendon length l_i^{mt} is obtained by regressing equations using the upper limb model [27], and k_i is a scale coefficient to address the subject-specificity. ϕ_i is the pennation angle between muscle fibre

and tendon. The tendon compliance is omitted for real-time computation. The muscle-tendon force is computed by:

$$\begin{aligned} F_i^{mt} &= (F_{CE,i} + F_{PE,i}) \cos\phi_i \\ &= [F_{o,i}^m f_a(\bar{l}_{i,a}^m) f(\bar{v}_i) a_i(t) + F_{o,i}^m f_p(\bar{l}_i^m)] \cos\phi_i \end{aligned} \tag{3}$$

where $F_{CE,i}$ and $F_{PE,i}$ are the active force generated by muscle contraction and passive force generated by muscle stretch, respectively. $f_a(\bar{l}_{i,a}^m)$ and $f(\bar{v}_i)$ denote the force-length relationship and force-velocity relationship respectively. $F_{o,i}^m$ is the maximum isometric force. $\bar{l}_{i,a}^m$ is the normalization of muscle fibre length l_i^m with respect to the muscle activation and optimal music fibre length $l_{o,i}^m$ [28]. $\bar{l}_i^m$ denotes the ratio of muscle fibre length to the optimal muscle fibre length. The detailed expressions of $F_{CE,i}$ and $F_{PE,i}$ can be found in [29] and [26]. The wrist joint torque is then computed by:

$$\hat{\tau} = \sum_{i=1}^{5} r_i F_i^{mt} \tag{4}$$

where $\hat{\tau}$ represents the estimated joint torque during motion tasks. Moment arm r_i of each muscle is determined by the partial derivative of muscle-tendon length with respect to the joint angle.

To obtain the subject-specific characteristics of the muscular and skeletal properties, the parameters, including the optimal muscle fibre length $l_{o,i}^m$, tendon length l_i^t, maximum isometric force $F_{o,i}^m$ and optimal pennation angle $\phi_{o,i}$, the non-linear factor A, and scale coefficient k_i, are optimised by minimisation of the difference between the estimation and joint torque from the inverse dynamic. The default physiological parameters and optimised range are given in Table I. The parameter optimisation are conducted using the genetic algorithm in MATLAB offline. Once the parameters are obtained, the joint stiffness K_{joint} can be derived by:

$$K_{joint} = \sum_{i=1}^{5} (r_i^2 K_i^{mt} + \frac{\partial r_i}{\partial \theta} F_i^{mt}). \tag{5}$$

where K_i^{mt} indicates the stiffness of each muscle. The K_i^{mt} is obtained by:

$$K_i^{mt} = K_i^{CE} + K_i^{PE} \tag{6}$$

where K_i^{CE} and K_i^{PE} are the stiffness of the contractile element and parallel element, respectively. Inclusion of the elastic tendon, in which the numerical stiff equation increases the computation burden of the muscle-tendon model, hurdles the implementation of the EMG-driven model in real-time. Therefore, the tendon is assumed as a rigid element in this study, as the ratio of tendon slack length to muscle-fibre length is small in wrist muscles [28]. The K_i^{CE} is obtained by:

$$K_i^{CE} = \frac{\gamma a_i(t) F_{o,i}^m f_a(\bar{l}_{i,a}^m)}{l_{o,i}^m} \tag{7}$$

where γ is set to 23.4 [22]. The K_i^{PE} is calculated by the slope of the passive force-length relationship to account for the muscle fibre stiffness in absence of the muscle activation $a_i(t)$. In specific, the K_i^{PE} is obtained through:

$$K_i^{PE} = \begin{cases} 0.0751 F_{o,i}^m & \bar{l}_i^m < 1 \\ 6.32 F_{o,i}^m & \bar{l}_i^m \geq 1. \end{cases} \tag{8}$$

TABLE I
PARAMETERS SETTING IN THE EMG-DRIVEN MODEL

	Muscle	Default	Optimised Range		Muscle	Default	Optimised Range
F_o^m	FCR	407	±50%	l_o^m	FCR	0.062	±2.5%
	FCU	479			FCU	0.051	
	ECRL	337			ECRL	0.081	
	ECRB	252			ECRB	0.058	
	ECU	192			ECU	0.062	
	Muscle	**Default**	**Optimised Range**		**Muscle**	**Default**	**Optimised Range**
l_t	FCR	0.24	±5%	ϕ_o	FCR	0.05	±5%
	FCU	0.26			FCU	0.2	
	ECRL	0.24			ECRL	0.04	
	ECRB	0.22			ECRB	0.16	
	ECU	0.23			ECU	0.06	
A		-2	[-3,0.001]	k_i	all muscle	1	[0.9,1.2]

C. Control strategy

The proposed control strategy consists of a position controller and an admittance controller. The position controller is used to ensure the tracking performance for the trajectory tracking control that is implemented to guide the subject's wrist joint following the reference trajectory [30], [31]. The parameters K_p, K_i and K_d are well-tuned to minimise the tracking errors (K_p = 4.65; K_i = 0.0075; K_d = 0.00225), which results in the max error of 10% and root-mean-square error (RMSE) of $0.0129\,\mathrm{rad}$ respectively.

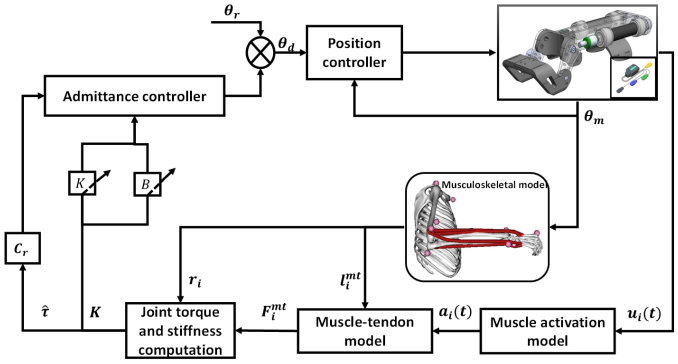

Fig. 2. The block diagram of the proposed adaptive control strategy for the wrist exoskeleton.

The admittance controller is utilised to determine the deviation of the trajectory in response to estimated joint torque. The transfer function of the admittance controller is written as:

$$\theta_d(s) = \theta_r(s) + \frac{C_r \hat{T}(s)}{Ms^2 + Bs + K} \tag{9}$$

where θ_d and θ_r are the desired trajectory and reference trajectory respectively. C_r is the cooperative ratio. $\hat{T}(s)$ denotes the joint torque obtained from the EMG-driven musculoskeletal

model. The M, B and K are the mass, damping and stiffness parameters of the admittance controller. Furthermore, the wrist exoskeleton should provide adjustable compliance to guarantee the safety during the rehabilitation exercise. This is achieved by relating the impedance model to the subjects' joint stiffness K_{joint}. The stiffness parameter K of the admittance controller is linearly adapted by:

$$K = K^{max} - (K^{max} - K^{min})\frac{K_{joint} - K_{joint}^{min}}{K_{joint}^{max} - K_{joint}^{min}} \tag{10}$$

the K^{max} and K^{min} are determined empirically, which are set to 10 and 3 respectively. The damping parameter B is shown that it has a linear relationship to K [32]. Therefore, in this study, the damping parameter is chosen as:

$$B = 0.2\sqrt{K}. \tag{11}$$

To avoid the instability of the control system and enhance safety, an additional saturation function is implemented.

D. Experimental Protocol

Twelve healthy subjects (aged between 27 and 30) participated in this study. Prior to the experiment, participation consent forms are signed by all subjects. All subjects have no reported wrist muscular disorders and can perform the wrist flexion/extension in full RoMs. This experiment is approved by the MaPS and Engineering Joint Faculty Research Ethics Committee of the University of Leeds (MEEC 18-002).

This first experiment is conducted to obtain the subject-specific EMG-driven model and to validate the estimated joint stiffness. To measure the EMG signal, electrodes (Delsys quattor sensor) are attached over four wrist muscles, including *Flexor Carpi Radialis* (FCR), *Flexor Carpi Ulnaris* (FCU), *Extensor Carpi Radialis*(ECR), *Extensor Carpi Ulnaris* (ECU). The raw EMG signal of ECR is assigned to the Extensor Carpi Radialis longus (ECRL) and Extensor Carpi Radialis Brevis (ECRB), as these two muscles are closely adjacent. The placement of electrodes is first based on the palpation. The qualities of the signal are evaluated through the Delsys data acquisition software. The sampling frequency is $2000\,\mathrm{Hz}$.

To record the motion data, two inertia measure units (IMUs) are attached to the third metacarpal bones and back of the forearm respectively. The sampling frequency is $256\,\mathrm{Hz}$. A Kalman filter is used to compute the wrist flexion/extension motion. Before the experiment, subjects are asked to perform the MVCs for muscle activation normalisation. Then subjects are asked to perform the continuous wrist flexion/extension motion for the subject-specific parameters optimisation. Each motion trial lasts $15\,\mathrm{seconds}$ and 2 trials are recorded. Since IMUs are sampled at $256\,\mathrm{Hz}$, all sensor data are resampled and synchronised at $1000\,\mathrm{Hz}$ for data processing.

The second experiment is conducted to evaluate the proposed adaptive cooperative control strategy. Three training protocols, namely, trajectory tracking control (TTC), fixed cooperative control (FCC), and adaptive cooperative control (ACC) are tested. For FCC and ACC, two different cooperative ratios are utilized to evaluate the performance. In specific, each training protocol is defined as,

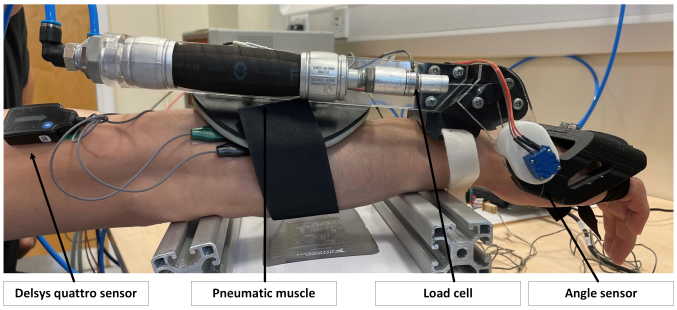

Fig. 3. Experiment setup. The wrist exoskeleton guides the subject's wrist following the predefined trajectory. The sEMG signal is recorded from the primary wrist muscles.

1) The first training protocol (TTC) is conducted without the cooperative control strategy (C_r = 0). The joint torque $\hat{\tau}$ and muscle activation levels $a_i(t)$ are monitored at the same time.
2) The second protocol (FCC) is conducted with the fixed admittance parameters, of which the M, K and B are set to 0.15, 10 and 0.63. Two cooperative ratio ($C_r = 0.3$ and 0.6) are used in FCC. In this experiment, the desired trajectory is determined by the estimated joint torque solely.
3) The third protocol (ACC) is conducted with the proposed adaptive control strategy. Two cooperative ratio ($C_r = 0.3$ and 0.6) are also utilised in the ACC. In this experiment, the robot's behaviour is regulated according to the estimated joint torque and joint stiffness.

During experiments, subjects are encouraged to involve their voluntary effort. The reference trajectory of all experiments is set as a sine-wave with the amplitude of $0.25\,\mathrm{rad}$ and frequency of $0.05\,\mathrm{Hz}$. In addition, the deviation is limited between $\pm 0.45\,\mathrm{rad}$, which is close to the maximum ROM of the wrist exoskeleton. Each protocol contains three trials and each trial lasts $60\,\mathrm{seconds}$. For all experiments, a five-minute rest is given between trials to prevent muscle fatigue.

E. Performance Index

Three performance indexes are evaluated, including RMSE, root-mean-square of estimated joint torque (RMS_τ), and root-mean-square of the deviation ($\mathrm{RMS}_{\mathrm{dev}}$). The RMSE between the desired trajectory (reference trajectory for TTC) and measured trajectory is calculated to evaluate the tracking performance. To compare the performance between different training protocols, the ratio of the RMS_τ and $\mathrm{RMS}_{\mathrm{dev}}$ is computed by:

$$r_{td} = \mathrm{RMS}_\tau / \mathrm{RMS}_{\mathrm{dev}} \tag{12}$$

where r_{td} represents the robot's compliance. In specific, a larger value means the wrist exoskeleton modifies the trajectory slightly, which indicates a smaller robot's compliance.

Separate one-way analysis of variance (ANOVAs) are conducted for each experiment. RMSE is used as the response

TABLE II
RESULTS OF JOINT STIFFNESS ESTIMATION ACROSS ALL SUBJECTS.

	Subject Index													
	S1	S2	S3	S4	S5	S6	S7	S8	S9	S10	S11	S12	Mean	Std.
Passive stiffness	0.81	0.43	0.41	0.19	0.21	0.55	1.17	2.22	0.83	0.64	0.83	1.06	0.78	0.55
Active stiffness	14.31	7.27	11.44	7.45	10.07	9.14	9.56	16.48	6.30	10.51	8.86	14.94	10.53	3.22

* Nm/rad.
* Active stiffness is calculated at neutral position with flexor activation of 15% MVC.
* Std. = standard deviation.

variable. A *post-hoc* analysis using Tukey's Honest Significant Difference test is applied. The significance level is set at $p < 0.05$.

III. RESULTS

A. Joint stiffness estimation

After optimisation, the personalised physiological parameters are used to estimate the joint stiffness based on equation (5). Additional, the parameters and MVCs are stored for further implementation in the proposed control strategy. In specific, the passive and active stiffness are validated by comparing with measurements in the literature respectively. The passive joint stiffness is simulated at the zero muscle activation level ($a_i(t) = 0$) and neutral position ($\theta_m = 0$). The active joint stiffness is emulated at the neutral position ($\theta_m = 0$) while the flexor are activated around 15% MVC ($a_{1,2}(t) = 0.15$), as reported in [33] and [34].

The results across all subjects are presented in Table II. The passive joint stiffness has a range from $0.21\,\mathrm{Nm/rad}$ to $2.22\,\mathrm{Nm/rad}$, while the active joint stiffness has a range from $7.45\,\mathrm{Nm/rad}$ to $16.48\,\mathrm{Nm/rad}$. The mean passive and active joint stiffness are 0.78 $\pm$ 0.55 Nm/rad and 10.53 $\pm$ 3.22 Nm/rad respectively. Fig. 4 elucidates the comparison of the passive joint stiffness with measurements in the literature. Table III gives the comparison between the model estimation and reported mean value under the same condition. Results yield that the estimated active stiffness has the similar value compared with [33], but slightly larger than [34].

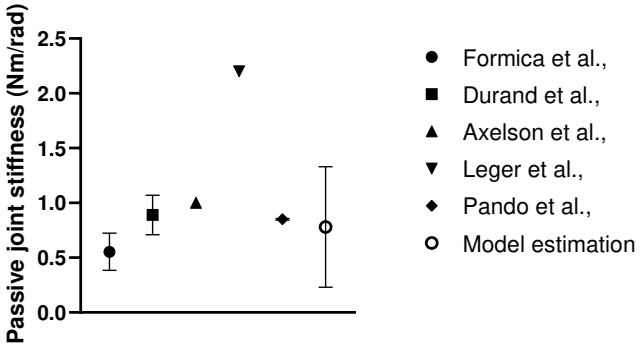

Fig. 4. Comparison of the estimated passive stiffness with measurements in the literature. Prior measurements has the range from $0.554\,\mathrm{Nm/rad}$ in [35], 0.89 $\pm$ 0.18 Nm/rad in [15],$0.554\,\mathrm{Nm/rad}$ in [36], $2.2\,\mathrm{Nm/rad}$ in [12] and 0.85 $\pm$ 0.007 Nm/rad in [13].

TABLE III
COMPARISON OF ACTIVE JOINT STIFFNESS WITH MEASUREMENTS IN THE LITERATURE.

Study	Contraction	Active stiffness	Model estimation
Halaki *et al.* [33]	Flexor	10.5 $\pm$ 0.4	10.53 $\pm$ 3.22
Milner *et al.* [34]	Flexor	9.22$\pm$ 6.60	10.53 $\pm$ 3.22

* Unit = Nm/rad (standard deviation)
* Active stiffness is calculated at neutral position with flexor activation of 15% MVC.

B. Adaptive cooperative control

1) Statistical results: Each experiment contains 36 trials ($n = 36$) for statistical analysis. Fig. 5 and Table IV give the results of performance indexes with respect to the different training protocols. The mean RMSE of TTC is 0.0264 $\pm$ 0.008 rad. The *post-hoc* tests show that TTC is significantly different from other experiments ($p < 0.001$). The mean RMSE are 0.0172 $\pm$ 0.002 rad and 0.0171 $\pm$ 0.002 rad for FCC with 0.3 C_r and 0.6 C_r respectively. The mean RMSE are 0.0186 $\pm$ 0.002 rad and 0.0214 $\pm$ 0.006 rad for ACC with 0.3 C_r and 0.6 C_r respectively.

TABLE IV
MEAN RMSE (rad), RMS_τ (Nm), $\mathrm{RMS}_{\mathrm{dev}}$ (rad) AND THE RATIO FOR ALL TRAINING PROTOCOLS.

	TTC	**FCC (C_r=0.3)**	**FCC(C_r=0.6)**	**ACC(C_r = 0.3)**	**ACC(C_r=0.6)**
RMSE	0.0264	0.0172	0.0171	0.0186	0.0214
RMS_τ	0.316	0.382	0.353	0.392	0.431
$\mathrm{RMS}_{\mathrm{dev}}$	N/A	0.012	0.022	0.017	0.042
Ratior_{td}	N/A	32.870	16.435	25.093	11.711

The mean RMSE significantly decreases when the cooperative control strategies are applied. Small RMSEs are found in FCC with two different cooperative ratios are applied. However, no significant difference is found between FCC with two different cooperative ratios ($p = 1$). The ACC with 0.3 C_r is not significant different to ACC with 0.6 C_r ($p = 0.104$) and the FCC with 0.3 C_r ($p = 0.718$). However, there is a significant difference between ACC with 0.6 C_r and FCC with 0.6 C_r ($p = 0.002$).

The ratio of the RMS_τ and $\mathrm{RMS}_{\mathrm{dev}}$ is calculated for fixed cooperative control and adaptive cooperative control respectively. The FCC with 0.3 C_r has the largest r_{td} among training protocols (32.87). The ACC with 0.3 C_r also has a large r_{td} (25.09), but is smaller than the FCC with 0.3 C_r. In addition, the smallest r_{td} is found in ACC with 0.6

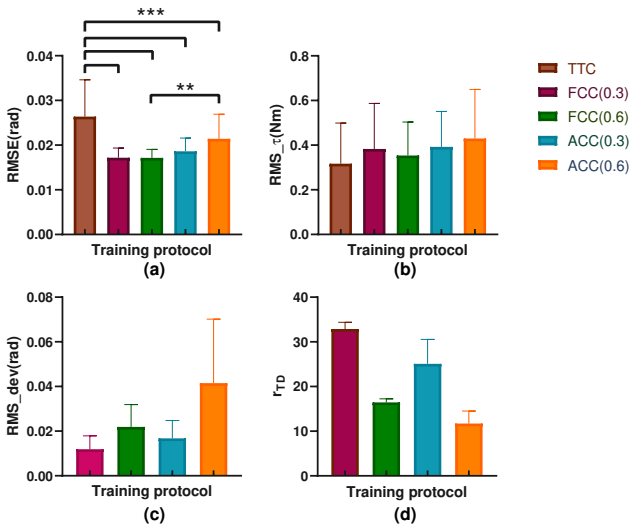

Fig. 5. Performance indexes of each training protocol. (a) RMSE; (b) RMS_τ; (c) $\mathrm{RMS}_{\mathrm{dev}}$; (d) The ratio of RMS_τ and $\mathrm{RMS}_{\mathrm{dev}}$.

C_r (11.71), compared with FCC with 0.6 C_r (16.44). This indicates the wrist exoskeleton becomes more compliant when the wrist joint stiffness is taken into account. Fig. 6 illustrates the exoskeleton's behaviour in each training protocol when the subject produces the voluntary effort. The similar joint torque output of one representative subject in wrist flexion direction is chosen.

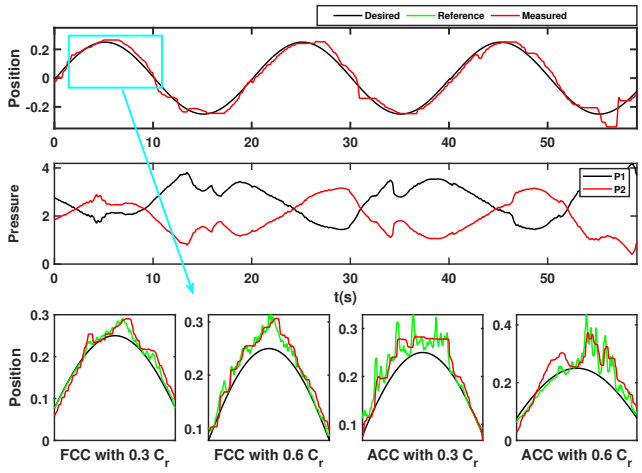

Fig. 6. Representative example of the exoskeleton's behaviour in each training protocol. The top figure shows the tracking performance of TTC when the subject actively participated. The middle figure indicates the input pressures. The bottom figures indicate the trajectory deviations in training protocols.

Fig. 7(a) and Fig. 7(b) illustrate the tracking performance of the ACC with two different cooperative ratios. The RMSE are $0.0174\,\mathrm{rad}$ and $0.0255\,\mathrm{rad}$ when the cooperative ratio is set to 0.3 and 0.6 respectively. The real-time adaptation of admittance parameters is also presented in the figure. In the third training protocol, stiffness and damping parameters increase as muscular efforts decrease while parameters decrease as muscular efforts increase. These parameters are also affected by the joint position. For example, at around $10\,\mathrm{second}$ of Fig. 7(a), the reference trajectory deviates more in flexion. In Fig. 7(b), the exoskeleton reaches a larger deviation when a larger cooperative ratio is used.

IV. Discussion

A. Joint stiffness estimation

The passive and active joint stiffness are derived through the EMG-driven musculoskeletal model. To evaluate the estimated joint stiffness, we compare the model estimation with the measurements reported in the literature which are obtained through the perturbation approaches. In specific, the passive joint stiffness is determined by the passive torque-angle curve, i.e., the wrist joint is passively driven from the neutral position to the certain RoMs. Likewise, the active joint stiffness is determined with the external perturbation, i.e., the position perturbations are applied to the wrist joint while the subject maintains a constant level of torque or EMG level [37]. The regression algorithms are then utilised to infer the relationship between muscle activities, joint position, and joint impedance.

For the passive stiffness, the model estimation has the mean value of 0.78 ± 0.55 Nm/rad. Prior studies reported the passive stiffness in wrist flexion/extension range from $0.554\,\mathrm{Nm/rad}$ (toward flexion) and $1.021\,\mathrm{Nm/rad}$ (toward extension) in [35], 0.89 ± 0.18Nm/rad in [15], $0.554\,\mathrm{Nm/rad}$ in [36], $2.2\,\mathrm{Nm/rad}$ in [12] and 0.85 ± 0.007 Nm/rad in [13]. The estimated passive joint stiffness in this study is within the middle range of the reported value. Likewise, the active stiffness is compared with [34] and [33]. The estimated joint stiffness is consistent with measurements from the literature. Furthermore, the age group reported in the literature, either for passive or active joint stiffness, covers the age group tested in this study. The results reveal that the EMG-driven musculoskeletal model shows the capability to interpret the wrist joint impedance during the motion tasks.

It is noticed that the optimised trial for each subject does not exceed the limits of the wrist's RoMs, in which passive stiffness is mainly characterised by the stretch of muscle tissues [34]. The active joint stiffness is dominated by the muscle contraction. This study emulates the active stiffness at the neutral position. The active stiffness varies over the wrist's RoM. This can be explained by the active force-length curve in response to the variability of the muscle fibre length during motion tasks. Additionally, the muscle co-contractions contribute to the active joint stiffness significantly, which is caused by the increased number of cross bridges [38]. The joint stiffness varies across the subjects, which has the range from $0.21\,\mathrm{Nm/rad}$ to $2.22\,\mathrm{Nm/rad}$ and $7.45\,\mathrm{Nm/rad}$ to $16.48\,\mathrm{Nm/rad}$ for passive stiffness and active stiffness respectively. The large variation can be explained by the optimised muscular parameters in the EMG-driven musculoskeletal model, such as the maximum isometric force, tendon slack length, and muscle-tendon length. The kinematic data is used to optimise these parameters which may lead to estimation errors. It is difficult to measure the dynamic joint torque when the exoskeleton is donned, due to the inherent compliance of the pneumatic actuators. Future work will carry

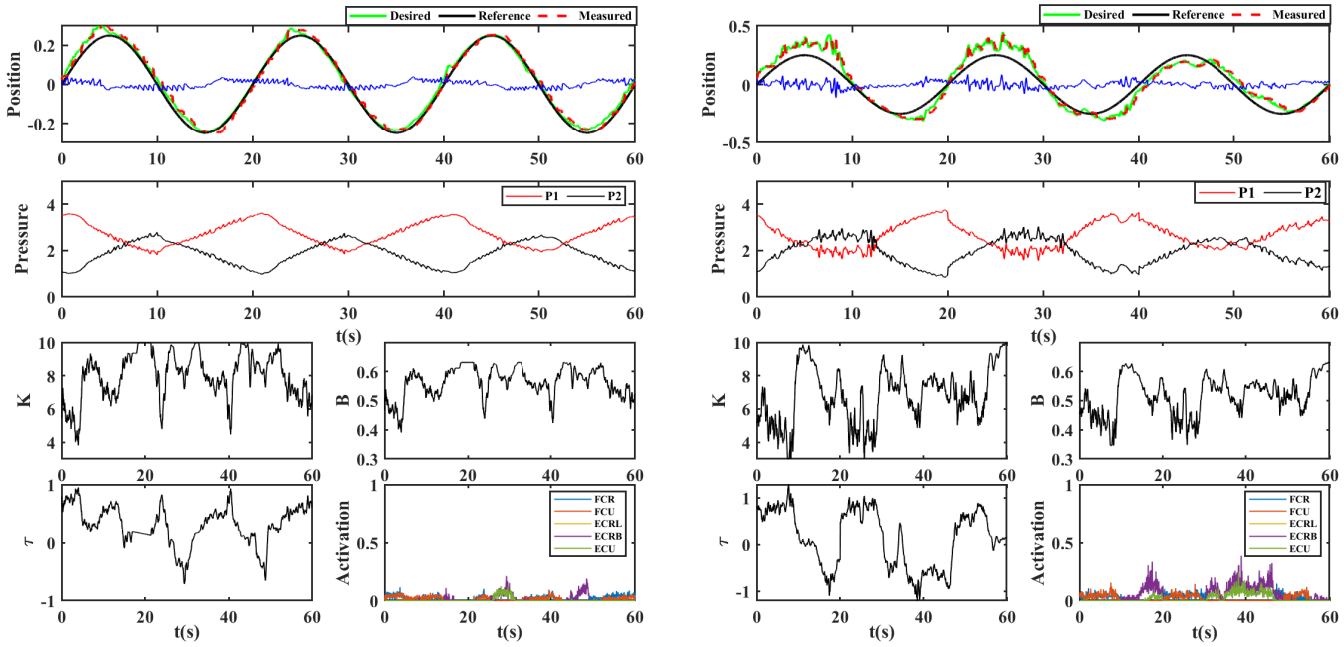

Fig. 7. Representative examples of the adaptive cooperative strategy with two different cooperative ratios. (a) For ACC with $0.3C_r$ (left), the RMSE is $0.0174\,\mathrm{rad}$. RMS_τ and $\mathrm{RMS}_{\mathrm{dev}}$ are $0.445\,\mathrm{Nm}$, and $0.021\,\mathrm{rad}$. (b) For ACC with $0.6C_r$ (right), the RMSE is $0.0255\,\mathrm{rad}$. RMS_τ and $\mathrm{RMS}_{\mathrm{dev}}$ are $0.633\,\mathrm{Nm}$ and $0.074\,\mathrm{rad}$ respectively.

out to apply a rigid apparatus to obtain the subject-specific muscular parameters in the model.

Understanding the joint impedance of the patient is essential for the assessment of motor function disorders after stroke [39], [40]. One of the most prevalent symptoms and a key source of impairment is the increased joint stiffness [35]. This may be due to the alteration of the intrinsic muscle properties, resulting in the abnormal joint stiffness [14]. The methods used to evaluate the subject's joint stiffness provide the vital information for robot-aided therapy. In another word, the estimated joint stiffness not only can be used to facilitate the clinical assessment and the evaluation of therapeutic efficacy but also can be conducive to the interactive training scheme. However, the regression algorithms used in the prior studies are difficult for real-time implementation. Rich and diverse experimental data are required to establish the relationship between stiffness, joint position, and muscle activation. The proposed method provides a feasible solution to the real-time computation of joint stiffness.

B. Adaptive cooperative control

To improve rehabilitation efficacy and safety, the adaptive cooperative control strategy is proposed. During the repetitive motion exercise, the EMG-driven musculoskeletal model continuously evaluates the muscular effort and joint impedance. The wrist exoskeleton's response is then adaptively regulated with respect to the joint impedance. The mean RMSE of TTC is significantly greater than in other experiments when the subject actively participates in the experiment, as shown in Fig. 5(a). This can be explained by the backdrivability of the pneumatic actuated wrist exoskeleton, which ensures safety in rehabilitation but leads to large tracking errors. Eventually, it may cause discomfort or injury to the wrist joint if the robot still follows the reference trajectory.

To evaluate the performance of the proposed ACC, the effects of FCC and ACC are compared with the different C_r. The r_{TD} shows that the exoskeleton becomes more compliant in ACC in both ratios when compared with FCC. Statistical results show that the mean RMSEs are similar to two C_rs in FCC, but a larger deviation is found when a higher ratio is applied. Moreover, it is found that the ACC has increased RMSE compared with FCC in the corresponding C_rs. This may be caused by the selection of the stiffness parameters, which leads to large compliance at the minimum stiffness parameter. The wrist exoskeleton provides the largest RoMs when the cooperative ratio is set to 0.6 in ACC. This reveals that the proposed ACC mainly takes account of the minimisation of the tracking errors under a small cooperative ratio. In contrast, the exoskeleton becomes more compliant to ensure safety when the cooperative ratio is set to a large value. The proposed ACC presents advantages compared with FCC based on the fact that the robot is capable of adapting the compliance according to wrist joint stiffness. This increases the robot's backdrivability in the training while maintaining adequate tracking performance.

The tracking error could be alleviated by employing the Euler-Lagrange system for the exoskeleton. For example, Roy *et al.* proposed the adaptive sliding mode control and the time-delayed adaptive-robust control for the Euler-Lagrange system to improve the effectiveness and robustness of trajectory tracking [41], [42]. Moreover, Zhao *et al.* proposed the optimisation-based control and the multi-domain hybrid model for the lower-limb prostheses to reduce the tracking error and improve energy efficiency [43]. Liang *et al.* proposed

the energy-based control for the 2-link PAM actuated robot to achieve accurate trajectory tracking control [44]. Nevertheless, the paper aims at designing the high-level controller that combines the EMG-driven musculoskeletal model and control strategy to enhance the safety and effectiveness of robot-aided wrist rehabilitation.

C. Muscle Models

The Hill's muscle model used in this paper is a static model. Nevertheless, this model contains many subject-specific physiological parameters that are well-tuned for each subject. The optimised model can interpret the subject's muscular efforts and joint impedance profiles simultaneously. Moreover, the stiffness and damping parameters in the proposed control strategy are dynamically varied in relation to the joint impedance.

There are other muscle models are used to describe and identify the dynamic properties of the musculoskeletal system based on the spring-damping system. The springs and dampers are utilised to interpret the stiffness and viscosity of the muscle fibre whereas the contractile element and passive parallel element are used in the Hill's muscle model. Moreover, the value of springs and dampers is determined by fitting the model response to experimental observations during the external perturbation. In contrast, the nominal physiological parameters in Hill's muscle model are obtained from cadavers' measurements and then personalised for each subject based on optimisation algorithms. In addition, it is found that the spring-damper system may not describe the fundamental dynamic properties of the musculoskeletal system, i.e., the non-linear force-length-velocity relationship in the Hill's muscle model, and it is sensitive to the measurement error [45].

D. Limitations and Future work

There are several limitations in the current study. Firstly, this study is experimentally validated only on healthy subjects. We will recruit more subjects, including patients with neurological diseases, to investigate and evaluate the proposed model-based joint impedance estimation method and control strategy. Secondly, this study utilises the PID controller for the trajectory tracking. We will carry on improving the tracking performance by employing pneumatic muscle modelling techniques and Euler-Lagrange dynamics. Finally, EMG-driven models will be employed to design more interactive control strategies for the robot-aided wrist rehabilitation.

V. Conclusion

This paper proposes the adaptive cooperative control strategy for the wrist rehabilitation exoskeleton using the model-based estimation method. To the authors' best knowledge, this is the first time to effectively combine the EMG-driven model-based approach and the interactive control strategy for the robot-aided wrist rehabilitation. Experimental evaluation conducted on 12 healthy subjects affirms the mean passive joint stiffness and active stiffness fall into the middle range of measurements reported in the literature. The adaptive cooperative control strategy is proposed that adaptively regulates exoskeleton's response with respect to the voluntary muscular efforts and joint impedance profile. Experimental results show that ACC outperforms other training protocols. The proposed adaptive cooperative control strategy shows the potential to enhance the training efficacy and safety for robot-aided wrist rehabilitation.

References

[1] S. Hussain, P. K. Jamwal, P. Van Vliet, and M. H. Ghayesh, "State-of-the-art robotic devices for wrist rehabilitation: Design and control aspects," *IEEE Trans Hum Mach Syst*, vol. 50, no. 5, pp. 361–372, 2020.

[2] E. T. Wolbrecht, V. Chan, D. J. Reinkensmeyer, and J. E. Bobrow, "Optimizing compliant, model-based robotic assistance to promote neurorehabilitation," *IEEE Trans. Neural Syst. Rehab. Eng.*, vol. 16, no. 3, pp. 286–297, 2008.

[3] A. U. Pehlivan, D. P. Losey, and M. K. O'Malley, "Minimal assist-as-needed controller for upper limb robotic rehabilitation," *IEEE Trans. Robot.*, vol. 32, no. 1, pp. 113–124, 2015.

[4] I. Jammeli, A. Chemori, H. Moon, S. Elloumi, and S. Mohammed, "An assistive explicit model predictive control framework for a knee rehabilitation exoskeleton," *IEEE ASME Trans Mechatron*, 2021.

[5] K. Gui, H. Liu, and D. Zhang, "A practical and adaptive method to achieve EMG-based torque estimation for a robotic exoskeleton," *IEEE ASME Trans Mechatron*, vol. 24, no. 2, pp. 483–494, 2019.

[6] I. L. Petersen, W. Nowakowska, C. Ulrich, and L. N. A. Struijk, "A novel sEMG triggered FES-hybrid robotic lower limb rehabilitation system for stroke patients," *IEEE Trans. Med. Robot. Bionics*, vol. 2, no. 4, pp. 631–638, 2020.

[7] L. Bi, C. Guan *et al.*, "A review on EMG-based motor intention prediction of continuous human upper limb motion for human-robot collaboration," *Biomed Signal Process Control*, vol. 51, pp. 113–127, 2019.

[8] M. Sierotowicz, N. Lotti, L. Nell, F. Missiroli, R. Alicea, X. Zhang, M. Xiloyannis, R. Rupp, E. Papp, J. Krzywinski *et al.*, "EMG-driven machine learning control of a soft glove for grasping assistance and rehabilitation," *IEEE Robot. Autom. Lett.*, vol. 7, no. 2, pp. 1566–1573, 2022.

[9] Q. Wu and Y. Chen, "Development of an intention-based adaptive neural cooperative control strategy for upper-limb robotic rehabilitation," *IEEE Robot. Autom. Lett.*, vol. 6, no. 2, pp. 335–342, 2020.

[10] M. Sharifi, A. Zakerimanesh, J. K. Mehr, A. Torabi, V. K. Mushahwar, and M. Tavakoli, "Impedance variation and learning strategies in human-robot interaction," *IEEE Trans Cybern*, pp. 1–14, 2021.

[11] Y. Zhu, Q. Wu, B. Chen, D. Xu, and Z. Shao, "Design and evaluation of a novel torque-controllable variable stiffness actuator with reconfigurability," *IEEE ASME Trans Mechatron*, 2021.

[12] A. B. Leger and T. E. Milner, "Passive and active wrist joint stiffness following eccentric exercise," *Eur. J. Appl. Physiol.*, vol. 82, no. 5, pp. 472–479, 2000.

[13] A. L. Pando, H. Lee, W. B. Drake, N. Hogan, and S. K. Charles, "Position-dependent characterization of passive wrist stiffness," *IEEE Trans. Biomed. Eng.*, vol. 61, no. 8, pp. 2235–2244, 2014.

[14] K. Park, P.-H. Chang, and S. H. Kang, "In vivo estimation of human forearm and wrist dynamic properties," *IEEE Trans. Neural Syst. Rehab. Eng.*, vol. 25, no. 5, pp. 436–446, 2016.

[15] S. Durand, C. P.-Y. Rohan, T. Hamilton, W. Skalli, and H. I. Krebs, "Passive wrist stiffness: the influence of handedness," *IEEE Trans. Biomed. Eng.*, vol. 66, no. 3, pp. 656–665, 2018.

[16] K. Kiguchi and Y. Hayashi, "An EMG-based control for an upper-limb power-assist exoskeleton robot," *IEEE Transactions on Systems, Man, and Cybernetics, Part B (Cybernetics)*, vol. 42, no. 4, pp. 1064–1071, 2012.

[17] L. Peternel, N. Tsagarakis, and A. Ajoudani, "A human–robot co-manipulation approach based on human sensorimotor information," *IEEE Trans. Neural Syst. Rehab. Eng.*, vol. 25, no. 7, pp. 811–822, 2017.

[18] C. W. Antuvan and L. Masia, "Position and stiffness modulation of a wrist haptic device using myoelectric interface," in *2017 International Conference on Rehabilitation Robotics (ICORR)*. IEEE, 2017, pp. 734–739.

[19] R. Wu, H. Zhang, T. Peng, L. Fu, and J. Zhao, "Variable impedance interaction and demonstration interface design based on measurement of arm muscle co-activation for demonstration learning," *Biomed Signal Process Control*, vol. 51, pp. 8–18, 2019.

[20] C. Zeng, C. Yang, H. Cheng, Y. Li, and S.-L. Dai, "Simultaneously encoding movement and sEMG-based stiffness for robotic skill learning," *IEEE Trans. Industr. Inform.*, vol. 17, no. 2, pp. 1244–1252, 2020.

[21] S. Pfeifer, H. Vallery, M. Hardegger, R. Riener, and E. J. Perreault, "Model-based estimation of knee stiffness," *IEEE Trans. Biomed. Eng.*, vol. 59, no. 9, pp. 2604–2612, 2012.

[22] A. Zonnino and F. Sergi, "Model-based analysis of the stiffness of the wrist joint in active and passive conditions," *J. Biomech. Eng.*, vol. 141, no. 4, 2019.

[23] W. Meng, B. Sheng, M. Klinger, Q. Liu, Z. Zhou, and S. Q. Xie, "Design and control of a robotic wrist orthosis for joint rehabilitation," in *2015IEEE/ASME Int. Conf. Adv. Intell. Mechatron. AIM*. IEEE, 2015, pp. 1235–1240.

[24] Y. Cao, Z. Fu, M. Zhang, and J. Huang, "Extended-state-observer-based super twisting control for pneumatic muscle actuators," vol. 10, no. 2. MDPI, 2021, p. 35.

[25] K. Qian, Z. Li, S. Chakrabarty, Z. Zhang, and S. Q. Xie, "Robust iterative learning control for pneumatic muscle with uncertainties and state constraints," *IEEE Trans. Ind. Electron.*, 2022.

[26] T. S. Buchanan, D. G. Lloyd, K. Manal, and T. F. Besier, "Neuromusculoskeletal modeling: estimation of muscle forces and joint moments and movements from measurements of neural command," *J. Appl. Biomech.*, vol. 20, no. 4, pp. 367–395, 2004.

[27] K. R. Saul, X. Hu, C. M. Goehler, M. E. Vidt, M. Daly, A. Velisar, and W. M. Murray, "Benchmarking of dynamic simulation predictions in two software platforms using an upper limb musculoskeletal model," *Comput Methods Biomech Biomed Engin*, vol. 18, no. 13, pp. 1445–1458, 2015.

[28] F. E. Zajac, "Muscle and tendon: properties, models, scaling, and application to biomechanics and motor control." *Crit Rev Biomed Eng*, vol. 17, no. 4, pp. 359–411, 1989.

[29] D. G. Lloyd and T. F. Besier, "An EMG-driven musculoskeletal model to estimate muscle forces and knee joint moments in vivo," *J. Biomech.*, vol. 36, no. 6, pp. 765–776, 2003.

[30] K. X. Khor, P. J. H. Chin, C. F. Yeong, E. L. M. Su, A. L. T. Narayanan, H. A. Rahman, and Q. I. Khan, "Portable and reconfigurable wrist robot improves hand function for post-stroke subjects," *IEEE Trans. Neural Syst. Rehab. Eng.*, vol. 25, no. 10, pp. 1864–1873, 2017.

[31] D. Buongiorno, E. Sotgiu, D. Leonardis, S. Marcheschi, M. Solazzi, and A. Frisoli, "Wres: a novel 3 dof wrist exoskeleton with tendon-driven differential transmission for neuro-rehabilitation and teleoperation," *IEEE Robot. Autom. Lett.*, vol. 3, no. 3, pp. 2152–2159, 2018.

[32] H. Gomi and R. Osu, "Task-dependent viscoelasticity of human multijoint arm and its spatial characteristics for interaction with environments," *J. Neurosci.*, vol. 18, no. 21, pp. 8965–8978, 1998.

[33] M. Halaki, N. O'Dwyer, and I. Cathers, "Systematic nonlinear relations between displacement amplitude and joint mechanics at the human wrist," *J. Biomech.*, vol. 39, no. 12, pp. 2171–2182, 2006.

[34] T. E. Milner and C. Cloutier, "Compensation for mechanically unstable loading in voluntary wrist movement," *Exp. Brain Res.*, vol. 94, no. 3, pp. 522–532, 1993.

[35] D. Formica, S. K. Charles, L. Zollo, E. Guglielmelli, N. Hogan, and H. I. Krebs, "The passive stiffness of the wrist and forearm," *J. Neurophysiol.*, vol. 108, no. 4, pp. 1158–1166, 2012.

[36] H. W. Axelson and K.-E. Hagbarth, "Human motor control consequences of thixotropic changes in muscular short-range stiffness," *J. Physiol.*, vol. 535, no. 1, pp. 279–288, 2001.

[37] A. C. Schouten, E. de Vlugt, J. B. van Hilten, and F. C. van der Helm, "Design of a torque-controlled manipulator to analyse the admittance of the wrist joint," *J. Neurosci. Methods*, vol. 154, no. 1-2, pp. 134–141, 2006.

[38] A. Klomp, J. H. De Groot, E. De Vlugt, C. G. Meskers, J. H. Arendzen, and F. C. Van Der Helm, "Perturbation amplitude affects linearly estimated neuromechanical wrist joint properties," *IEEE Trans. Biomed. Eng.*, vol. 61, no. 4, pp. 1005–1014, 2013.

[39] L.-Q. Zhang, J. Son, H.-S. Park, S. H. Kang, Y. Lee, and Y. Ren, "Changes of shoulder, elbow, and wrist stiffness matrix post stroke," *IEEE Trans. Neural Syst. Rehab. Eng.*, vol. 25, no. 7, pp. 844–851, 2017.

[40] E. de Vlugt, H. J. van der Krogt, Á. Helgadóttir, J. H. Arendzen, C. G. Meskers, J. H. de Groot *et al.*, "Estimation of tissue stiffness, reflex activity, optimal muscle length and slack length in stroke patients using an electromyography driven antagonistic wrist model," *Clinical Biomechanics*, vol. 35, pp. 93–101, 2016.

[41] S. Roy, S. B. Roy, J. Lee, and S. Baldi, "Overcoming the underestimation and overestimation problems in adaptive sliding mode control," *IEEE/ASME Trans. Mechatron.*, vol. 24, no. 5, pp. 2031–2039, 2019.

[42] S. Roy, J. Lee, and S. Baldi, "A new adaptive-robust design for time delay control under state-dependent stability condition," *IEEE Trans. Contr. Syst. Technol.*, vol. 29, no. 1, pp. 420–427, 2020.

[43] H. Zhao, J. Horn, J. Reher, V. Paredes, and A. D. Ames, "Multicontact locomotion on transfemoral prostheses via hybrid system models and optimization-based control," *IEEE Trans. Autom. Sci. Eng.*, vol. 13, no. 2, pp. 502–513, 2016.

[44] D. Liang, N. Sun, Y. Wu, Y. Chen, Y. Fang, and L. Liu, "Energy-based motion control for pneumatic artificial muscle actuated robots with experiments," *IEEE Trans. Ind. Electron.*, vol. 69, no. 7, pp. 7295–7306, 2021.

[45] D. A. Kistemaker and L. A. Rozendaal, "In vivo dynamics of the musculoskeletal system cannot be adequately described using a stiffness-damping-inertia model," *PloS one*, vol. 6, no. 5, p. e19568, 2011.

Yihui Zhao received BEng and MS degrees both in Electrical and Electronic Engineering from the University of Leeds, Leeds, United Kingdom, in 2016 and 2017, respectively. He is currently pursuing the Ph.D. degree with the School of Electrical and Electronic Engineering, University of Leeds. His research interests include musculoskeletal modelling, and myoelectric control for rehabilitation robotics.

Sheng Bo received the M.Eng. degree in mechatronics from the Huazhong University of Science and Technology, China, in 2014, and the Ph.D. degree in mechanical engineering from the University of Auckland, New Zealand, in 2019. He was a Research Associate with the Department of Exercise Sciences, the University of Auckland, from 2019 to 2021. He is currently a Lecturer with the School of Mechatronic Engineering and Automation, Shanghai University. He has participated in over ten research projects in areas of rehabilitation robots, interaction control, and medical informatics. He is the author of over 26 academic journal and conference papers. His research interests include robot-assisted rehabilitation, human–robot interaction, and medical informatics

Kun Qian received a BEng degree in Electrical and Electronic Engineering and a MS degree in Digital Communication Network both from the University of Leeds, Leeds, United Kingdom, in 2016 and 2017, respectively. He is currently pursuing the Ph.D. degree with the School of Electrical and Electronic Engineering, University of Leeds. His research interests include iterative learning control, and advanced control strategies for rehabilitation robotics.

Zhiqiang Zhang received the Ph.D. degree in electrical engineering from the University of Chinese Academy of Sciences, Beijing, China, in 2010. He was a research associate in Imperial College London for five and half years. He is an Associate Professor in body sensor networks for healthcare and robotic control with the University of Leeds, Leeds, U.K. His primary research interests are human kinematics, musculoskeletal modelling, and machine learning. He has more than 50 papers in peer-reviewed publications.

Zhenhong Li received a BEng degree in electrical engineering from Huazhong University of Science and Technology, Hubei, China, and MS and PhD degrees in control engineering from the University of Manchester, Manchester, United Kingdom, in 2014 and 2019, respectively. He is now a research fellow in the School of Electronic and Electrical Engineering at the University of Leeds. From 2018 to 2019, he was a research associate at the University of Manchester, United Kingdom. His research interests include distributed optimization, and cooperative control of multi-agent systems.

Gu-Qiang Li received the MSc in sport body science from the Jiangsu Normal University. He is currently an Associate Professor with the School of Rehabilitation Medicine, Binzhou Medical University, Yantai, China. His research interests include rehabilitation robotics, intelligent rehabilitation assistive devices, and 3D-printed orthosis in the clinic.

Abbas Ali Dehghani-Sanij is currently a Professor of Bio-Mechatronics and Medical Robotics with the School of Mechanical Engineering, University of Leeds. His research interests include bio-robotics, intelligent control, sensors and actuators using integrated system design approach, where functional materials, sensors, actuators, and control are brought together to develop intelligent systems/devices. His research focus is mobility and intelligent control in robots and also development of devices to support mobility in patients and the growing ageing population, as well as wearable robotic systems for enhancing human capabilities. His current research includes design and development of intelligent robotic exoskeletons, soft robotics, and artificial limbs.

Shengquan Xie received the Ph.D. degree in mechanical engineering from the University of Canterbury, Christchurch, New Zealand, in 2002. He joined the University of Auckland in 2003 and became a Chair Professor in (Bio) mechatronics in 2011. Since 2017, he has been the Chair of robotics and autonomous systems with the University of Leeds, Leeds, U.K. He has authored or co-authored eight books, 15 book chapters, and more than 400 international journal and conference papers. His current research interests include medical and rehabilitation robots and advanced robot control. Prof. Xie is an elected Fellow of The Institution of Professional Engineers New Zealand.